Petroleum Science 21 (2024) 1396–1404

Contents lists available at ScienceDirect

Petroleum Science

journal homepage: www.keaipublishing.com/en/journals/petroleum-science

Original Paper

TBAB hydrate formation and growth in a microdevice under static and dynamic conditions

Xing-Xun Li [a, *], Ming Liu [a], Qing-Ping Li [b], Wei-Xin Pang [b], Guang-Jin Chen [a], Chang-Yu Sun [a]

[a] State Key Laboratory of Heavy Oil Processing, China University of Petroleum Beijing, Beijing, 102249, China
[b] State Key Laboratory of Natural Gas Hydrate, CNOOC Research Institute Co., Ltd., Beijing, 100027, China

ARTICLE INFO

Article history:
Received 15 January 2023
Received in revised form
6 April 2023
Accepted 28 September 2023
Available online 29 September 2023

Edited by Jia-Jia Fei and Min Li

Keywords:
Hydrate formation
Hydrate growth
Microdevice
In-situ measurement

ABSTRACT

The natural gas hydrate has become one of the most promising future green energy sources on the earth. The natural gas hydrates mostly exist in the sediments with porous structure, so a solid understanding of the hydrate formation and growth processes in the porous medium is of significance for the exploitation of natural gas hydrate. The micro-packed bed device is one of the efficient microfluidic devices in the engineering field, but it has been rarely used for the hydrate-based research. In this study, a transparent micro-packed bed device filled with glass beads was developed to mimic the porous condition of sediments, and used to in-situ visualize the hydrate formation and growth habits in the pore spaces under both static and dynamic conditions. For the static experiment, two types of hydrate growth patterns in porous medium were observed and identified in the micro-packed bed device, which were the grain-coating growth and pore-filling growth. For the dynamic condition, the hydrate formation, growth, distribution habits and hydrate blockage phenomena in the pore spaces were in-situ visually captured. The impacts of flowrate and subcooling on the pressure variation of the micro-packed bed and the duration of the hydrate growth under dynamic flow condition in pores were in-situ monitored and analyzed. The higher flowrate could result in the faster hydrate growth and more severe blockage in pores, but the effect of subcooling condition might be less significant at the high flowrate.

1. Introduction

The natural gas hydrate has become a new clean green energy with great promising developments in the near future (Makogon, 2010; Yin and Linga, 2019). The safe and efficient hydrate exploitation has been a crucial issue encountered for the effective utilization of this type of energy source. Hydrates mostly exist in sediments of the seafloor and frozen soil layer with porous structure, which are considered as being difficult for extraction (Gao, 2022). Thus, the investigations of hydrate formation and growth processes in the porous medium are of significant importance for the fundamental understanding of hydrate evolution in porous sediment and hence enhancing the hydrate exploitation efficiency.

In order to provide an in-situ direct visual investigation on the phase behavior, interfacial phenomenon, multiphase flow transport in porous media, the microfluidic technique has been regarded as a great tool in the energy-related field (Sinton, 2014), such as oil and gas area. Abedini et al. (2022) highlighted the current and future applications of the state-of-the-art microfluidic-based approach on the measurements of fluid phase and property in the energy sector. Lifton (2016) pointed out that the microfluidic devices can be used and accepted as a useful methodology for the visualization and investigation on the processes in the oil and gas industries, such as enhanced oil recovery. Fani et al. (2022) presented the significant role of microfluidic chip on the stimulation and visualization of the microscale processes of pore fluids and addressed the great potentials of microfluidics on the chemical enhanced oil recovery. Gunda et al. (2011) designed the microfluidic chip with porous structure to mimic the realistic pore network of the reservoir rock and carried out the waterflooding experiments in the microchip, and demonstrated the feasibility of the conception of “Reservoir-on-a-Chip” in the reservoir engineering area. Lin et al. (2016) studied and directly visualized the dynamics of the deposition of

* Corresponding author.
E-mail address: lixingxun@cup.edu.cn (X.-X. Li).

https://doi.org/10.1016/j.petsci.2023.09.024

asphaltene particles at a pore scale in a microfluidic chip with porous structure, investigating the impact of asphaltene solubility on deposition. Tetteh et al. (2021) used a micromodel designed with the pore channel network to perform flow experiments to observe the fluid-fluid interactions in the process of the low salinity waterflooding. Behera et al. (2022) carried out pore-scale experiments on the oil displacement by nanofluid flooding in the glass microchip, investigated the oil-nanofluid-rock interaction behavior and the change of wetting condition of the rock surface. The microfluidic technique based on the lab-on-chip methodology have been effectively widely used for the phase behavior (Alfi et al., 2016; Guo et al., 2022; Mostowfi et al., 2012), emulsions (Lin et al., 2018; Zhao et al., 2022), coalescence (Dudek et al., 2020; Tian et al., 2022), wettability (Jafari and Jung, 2019; Saadat et al., 2021), flooding (Mahmoudzadeh et al., 2022; Mohammadi and Mahani, 2020; Zhao et al., 2020) and other relevant processes in the oil and gas industries.

In addition, recently, the microfluidic technique has started to be applied to the hydrate-related studies (Almenningen et al., 2021; Chen and Hartman, 2018; Chen et al., 2020; Ji et al., 2021; Li et al., 2022; Lv et al., 2021; Muraoka et al., 2020; Wang et al., 2021). For instance, Wang et al. (2021) used a microfluidic device to study the formation and dissociation processes of methane hydrate, and visualize the reformation of hydrate induced by the microbubbles. Muraoka et al. (2020) developed a two-dimensional glass micromodel to directly perform a microscopic observation on the hydrate formation behavior in the pore space and in-situ measure the water permeability. Pandey et al. (2022) carried out a pore-scale visual experiment on the CO_2 injection into CH_4 hydrate in a high-pressure model to obtain the characteristics of hydrate morphology evolution in the porous media.

Most of the microfluidic devices used in the micro-scale studies discussed above were two-dimensional microfluidic chip or micromodel etched with microchannels or porous structure. The microreactor technique have been enormously used for the in-situ reaction monitoring in terms of flow synthesis and chemistry (Sivo et al., 2021, 2022). The micro-packed bed is regarded as one of the useful and important microfluidic devices for the investigations on the mass transfer, hydrodynamics and reactions, merging the advantages of both microreactor and packed bed devices (Faridkhou et al., 2016). The micro-packed bed device has been mainly widely used in the area of hydrodynamics (Al-Rifai et al., 2016; Cao et al., 2021; Faridkhou and Larachi, 2014), reaction and catalyst (Cao et al., 2017; Farsi et al., 2020; Moulijn et al., 2016). However, the micro-packed bed device has been rarely used for the investigation on the hydrate-related studies. Thus, in this study, a transparent micro-packed bed device filled with glass beads for simulating the porous structure of hydrate-bearing sediment was developed to investigate the hydrate formation and growth habits in pore spaces. Moreover, most of previous microfluidic studies on the hydrate formation and hydrate film growth processes were carried out under the static condition. In this study, the hydrate formation and growth experiments were also performed under the dynamic flow condition, by considering the effects of flowrate and subcooling.

2. Experimental section

2.1. Materials

The deionized water and TBAB (tetrabutylammonium bromide) (Aladdin, ≥99%) were used to make the 10 wt% TBAB aqueous solution for the TBAB hydrate formation. In order to clearly in-situ observe the formation and growth processes of the hydrate in the porous medium, the transparent PMMA (polymethylmethacrylate) was used as the material of manufacturing the microdevice, and the glass beads were filled and packed as a single layer in the hydrate formation area of the microdevice to make the micro-packed bed device used in this study. Fig. 1 shows the schematic diagrams of the structure of the micro-packed bed device. The glass beads with a diameter of 1 mm were packed in the microdevice in the most densely packed form, and the depth of the microdevice was 1 mm. In order to prevent the glass beads from blocking the inlet and outlet channels of the microdevice and affecting the dynamic fluid flow, two baffles with the length of 1 mm and the width of 0.3 mm were set at the inlet and outlet channels of the microdevice (Fig. 1(a)). In order to avoid the problem of local supercooling around the clamping area of the clamper caused by the metal clamper, a threaded flange was designed to be fixed at the inlet and outlet of the microdevice, a PEEK (polyether ether ketone) joint was used to connect the microdevice and the pipeline, as shown in Fig. 1(b).

2.2. Methods

Fig. 2 shows the experimental setup for the hydrate formation and growth in a micro-packed bed device under static and dynamic conditions supported by the microfluidic technique and micro imaging technology. The experimental system consists of four parts: (1) Image acquisition and analysis system: it was composed of a computer, a CCD camera (TOUPCAM 5.1 MP) and a microscope (Changrong S-T). During the experiment, the microscopic image information during the formation and growth of hydrate could be collected, stored and analyzed by this system. (2) Temperature and pressure acquisition and control system: it was composed of a constant-temperature cooling water bath (HX-3008), data recorder (SIN-R200D), temperature sensor (PT-100), pressure transmitter (MIK-P300, 0–0.6 MPa). The experimental temperature was controlled by the constant-temperature cooling water bath. The temperature and pressure were collected by the temperature sensor and the pressure transmitter at both ends of the reactor and then sent to the data recorder. (3) Flow control system: it was composed of a microfluidic constant-flow syringe pump (LSP02-2A, Longer pump) and a piston syringe. During the experiment, the liquid was injected into the microdevice at the low flowrate by using the microfluidic constant-flow syringe pump. (4) Micro-packed bed device system: a single layer of glass beads was tightly packed in the microdevice to simulate the structure of the porous media and provide the pore space for the hydrate formation and growth at a pore scale.

In this study, considering the advantages of the microdevice, such as high-definition visibility, uniform heat transfer and accurate controlling of multiphase fluid at a microscale, the micro-packed bed was used to explore the formation and growth processes of TBAB hydrate under static and dynamic conditions. In this experiment, the ice-induced hydrate formation approach was employed to shorten the induction time required for the hydrate nucleation, which was used in our previous studies (Li et al., 2020, 2022). The hydrate was more likely to be formed in the process of ice melting. After increasing the temperature to decompose the hydrate, and then cooling down the temperature to the target experimental temperature below the equilibrium condition, the memory effect of hydrate can shorten the induction time of hydrate formation.

In order to ensure that the cooling and freezing durations in each run of the experiments were approximately the same, maintain the water bath temperature stable at the same temperature of

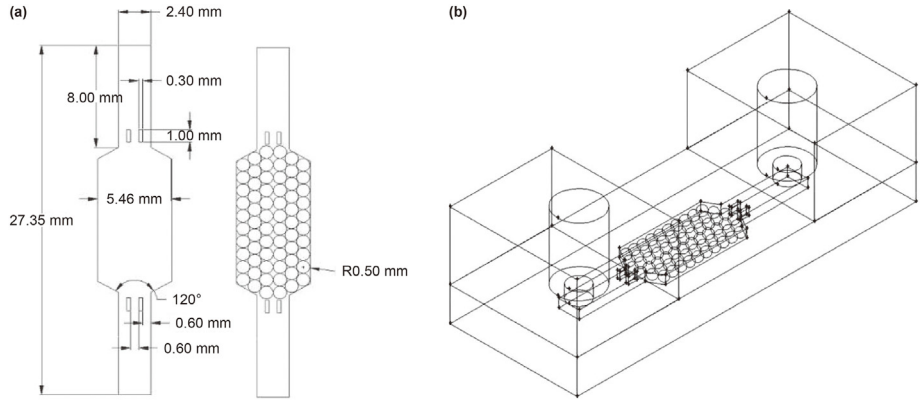

Fig. 1. Schematic diagrams of (**a**) two-dimensional structure and (**b**) two-dimensional structure of the micro-packed bed device.

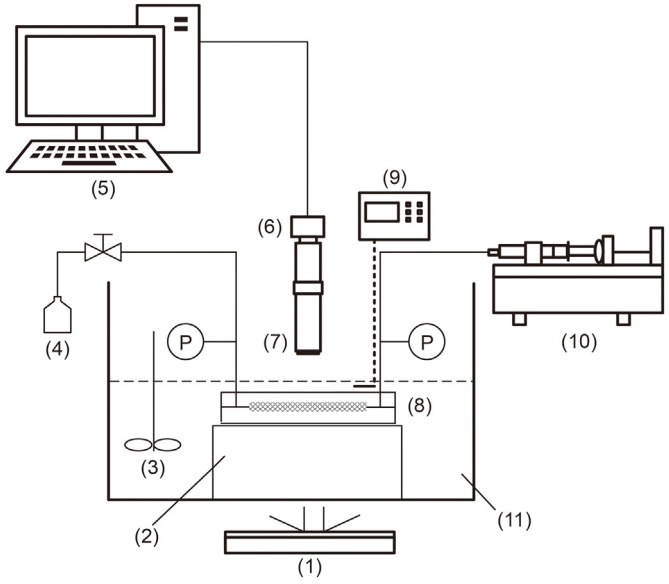

Fig. 2. The experimental setup for the formation and dissociation of hydrate in a micro-packed bed device: (1) light source, (2) micro-packed bed device support, (3) stirrer, (4) recovery tank, (5) computer, (6) CCD, (7) microscope, (8) micro-packed bed device, (9) temperature sensor and acquisition, (10) microfluidic syringe pump, (11) constant-temperature cooling water bath.

3 °C before the cooling in each experiment. The TBAB solution was then injected into the micro-packed bed device. The temperature was then reduced to below zero to freeze the solution in the micro-packed bed device. After the ice formation, the temperature was then elevated to 0 °C and stabilized for 15 min to ensure the hydrate formation in the microdevice. The temperature in the microdevice was then elevated and controlled at about 8 °C, which was above the phase equilibrium temperature of hydrate formed by 10 wt% TBAB (Oyama et al., 2005), in order to completely decompose the hydrate. For the hydrate formation experiment, the experimental temperature was cooled down to below the equilibrium temperature. For the static experiment, the microfluidic syringe pump was closed to keep the system at a steady state. For the dynamic flow experiment, the TBAB aqueous solution was injected into the micro-packed bed device at a low constant flowrate by the microfluidic syringe pump to mimic the seepage phenomenon in porous media. In order to investigate the effect of flowrate on the hydrate formation under dynamic condition, different flowrates ranging from 0.05 to 0.30 mL/min were used. To reveal the impact of subcooling on the hydrate formation under dynamic flow, the experiments at three different temperatures of 1, 2 and 3 °C were carried out in this study.

3. Results and discussion

3.1. Hydrate formation and growth behaviors in the micro-packed bed device under static condition

The formation and growth processes of TBAB hydrates in a micro-packed bed device were in-situ imaged and investigated under static condition. The experimental pressure was atmospheric pressure and the experimental temperature was 1 °C. Due to the different refractive indices of the hydrate crystal, the packed glass bead and the TBAB solution, a clear phase boundary could be observed when the hydrate was formed. During the experiment, the growth of hydrate can be visualized and recorded by capturing the evolution process of the boundary of the hydrate phase. The thickening growth process of hydrate can be evaluated by monitoring the reflection and refraction variations of the light during the growth process of hydrate.

Fig. 3 shows the growth process of TBAB hydrate in the micro-packed bed device under the static condition. Two hydrate growth habits were directly observed on the packed particles and in the porous spaces in the micro-packed bed device, which are grain-coating growth (the yellow dotted circle in Fig. 3) and pore-filling growth (the blue dotted circle in Fig. 3). Regarding the time of cooling to 1 °C as the time of $t = 0$ s, there was no hydrate observed in the micro-packed bed device at $t = 0$ s. At $t = 660$ s, small hydrate crystals are first observed on the edge of the glass beads, as shown in the Fig. 3(a). The hydrate tended to grow along the growth front of the crystal to the surface of the glass beads and covered the surface of the glass beads, behaved as the grain-coating growth pattern. At the same time, the hydrate also grew toward the pore space among grains to fill the pores, regarded as the pore-filling growth. At $t = 810$ s, the transparent flaky hydrate crystals can be clearly observed. At $t = 1680$ s, the hydrate crystals almost filled the glass bead pores where the hydrate was initially nucleated, and started to grow toward the adjacent pores. When $t = 2700$ s, it was observed that the hydrate almost filled the adjacent pores. From $t = 1680$ s to $t = 2700$ s, the hydrate grew rapidly in the pores and filled the pores of the adjacent glass beads. However, the hydrate did not grow significantly on the surface of the glass beads. The growth rate of hydrate on the glass beads was slower than that in the pores. This could be caused by the larger pore volume providing more effective contact area for the hydrate growing into the pores. From $t = 2700$ s to $t = 3600$ s, the lateral

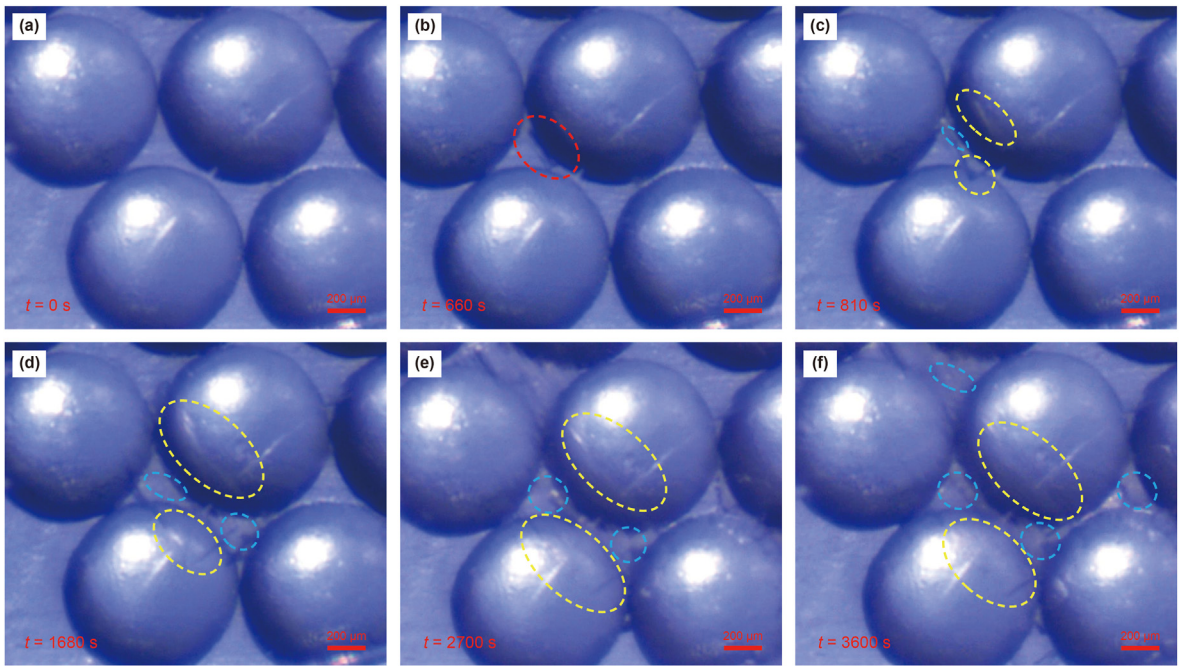

Fig. 3. TBAB hydrate growth process in a micro-packed bed device under static condition (colored dotted circles indicate the typical locations where the solid hydrate formed).

growth rate of hydrate became slow, but the hydrate thickening growth mainly occurred. After $t = 3600$ s, the size and morphology of hydrate crystals did not change further significantly.

3.2. Hydrate formation behavior in the micro-packed bed device under dynamic condition

In this section, the typical process of hydrate formation from TBAB solution in the micro-packed bed device was investigated under the dynamic flow condition. The TBAB solution passed through the micro-packed bed at a constant flow rate of 0.3 mL/min under the experimental conditions of atmospheric pressure and 1 °C. The formation of hydrate during the dynamic flow leaded to the change of porous condition in the micro-packed bed, and thereby resulted in the reduction of the permeability of the porous medium. Thus, as the hydrate was formed, the pressure difference between both ends of the micro-packed bed gradually increased during the constant flowing at a small flowrate of 0.3 mL/min.

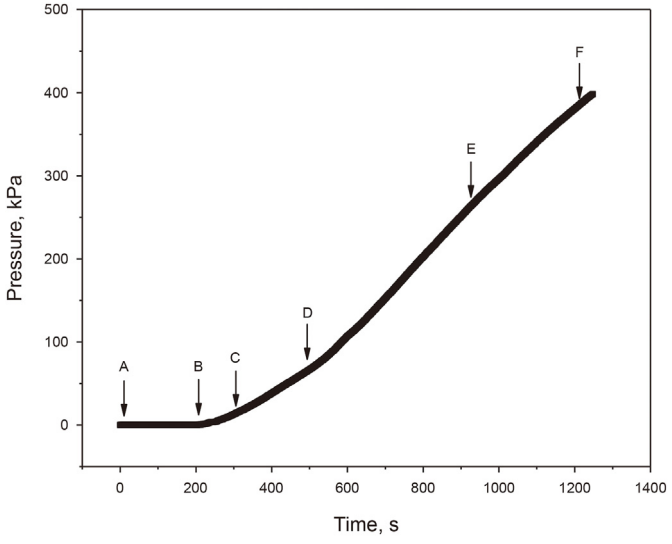

Fig. 4. Variation of pressure difference across the micro-packed bed with time at 1 °C and the flowrate of 0.3 mL/min.

Fig. 4 shows the variation trend of the pressure difference at both ends of the micro-packed bed. The differential pressure gradually increased with time during the dynamic flow condition. Point A in Fig. 4 is the starting time point when the TBAB solution was introduced into the micro-packed bed at a constant flow rate of 0.3 mL/min. With the formation of hydrate in the micro-packed bed device, the pressure difference between the two ends of the microdevice gradually increased. Point B is the time point when the pressure difference between the two ends of the microdevice began to be realized. Point D is the time point when the growth rate of the pressure difference at both ends of the reactor started to increase. Point C is a certain time point in the process (BD) from the point B to the point D. Point E is a certain time point in the process (DF) from the point D to the point F. According to the variation trend of differential pressure at both ends of the microdevice with time, the formation process of hydrate could be divided into three stages. The first stage (AB) is from point A to point B, in which the formation of hydrate did not cause the pressure difference change at both ends of the micro-packed bed. The second stage (BD) is from point B to point D, in which the formation of hydrate caused the gradual increase of the pressure difference at both ends of the micro-packed bed. The third stage (DF) is from point D to point F. In this stage, the pressure difference between the two ends of the micro-packed bed increased more significantly by a higher increasing rate. Both of the pressure differences at both ends of the micro-packed bed in the second stage (BD) and the third stage (DF) increased with the time linearly, but at different increasing rates. So there is a turning point D on the curve of the pressure difference changing with time.

Fig. 5(a)–(f) shows the microscopic images of the hydrate formation and growth processes in the three stages discussed above in the micro-packed bed device under the dynamic flow condition. For the convenience of observation, the positions of hydrate

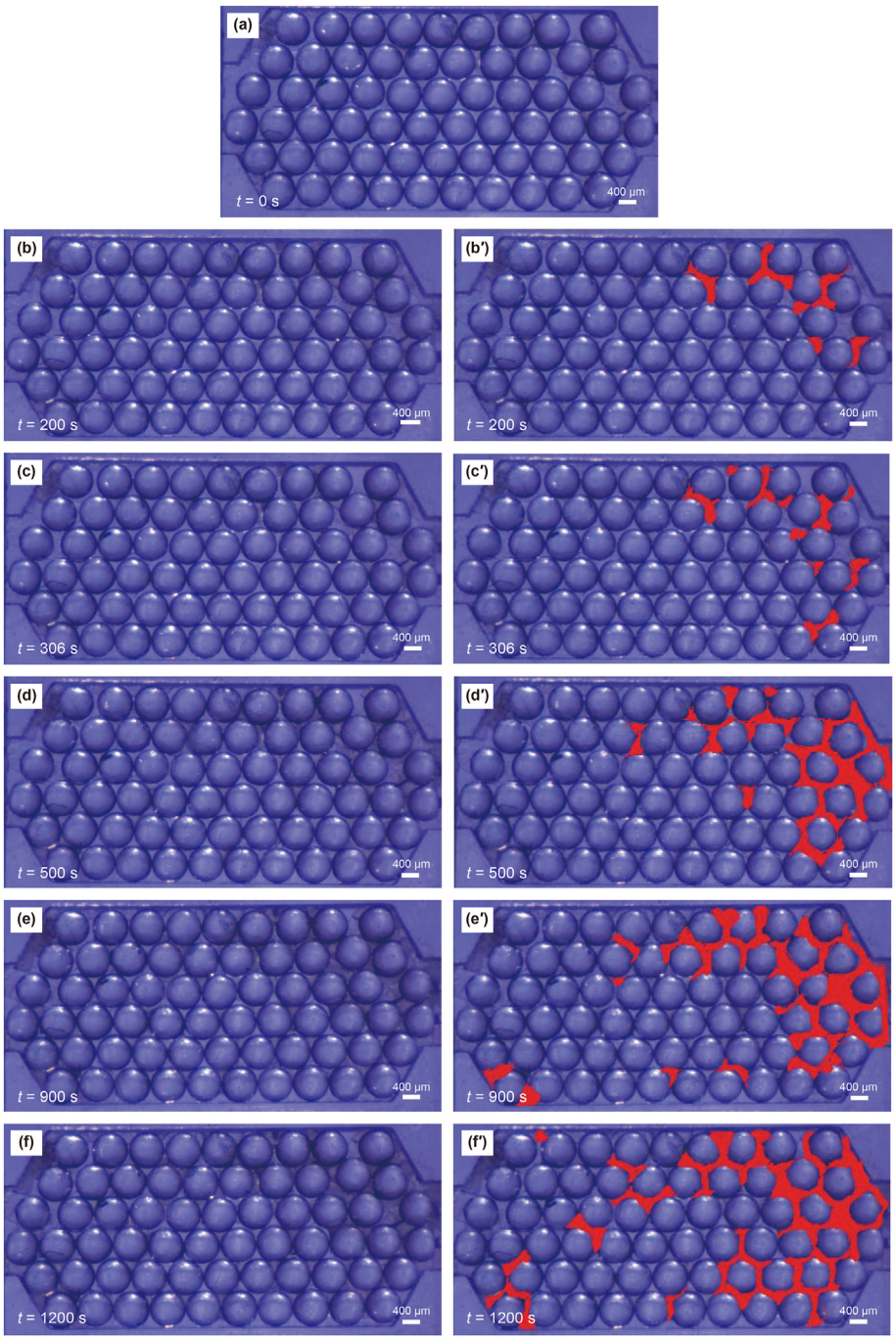

Fig. 5. Microscopic images of the hydrate formation process in the micro-packed bed device under dynamic flow condition at 1 °C and the flowrate of 0.3 mL/min (Fig. 5(**b**)–(**f**) are the original microscopic images, and Fig. 5(**b'**)–(**f'**) show the positions of hydrate formation in Fig. 5(**b**)–(**f**) correspondingly marked with red sign).

formation in Fig. 5(b)–(f) are correspondingly marked with red sign in Fig. 5(b')–(f'). In the first stage, it can be seen from the microscopic images Fig. 5(a) and (b) that the formation of hydrate gradually increased and started to fill the pores between glass beads in the micro-packed bed device. However, the amount of hydrate formed was not sufficient enough to cause the variation of the pressure difference at both ends of the micro-packed bed device. In the second stage, it can be seen from microscopic images Fig. 5(b) and (c) that the amount of hydrate formed continued to be gradually increased. From the microscopic images Fig. 5(c) and (d), it can be seen that the accumulation of the formed hydrate in the micro-packed bed gradually mainly caused the channel blockage at the outlet of the microdevice. At this time, the pressure difference at both ends of the microdevice gradually raised. In the third stage, it can be observed from the microscopic images Fig. 5(d) and (e) that the formation and growth of hydrate leaded to the decrease of refractive index, and the color of the region where hydrate formed becomes remarkably darker. Therefore, the hydrate thickening growth could mainly occur in the pores during this stage. From the microscopic images Fig. 5(e) and (f), it can be observed that the change of hydrate growth in the micro-packed bed was no longer remarkable. Before the time point of D, the outflow of fluid could be

observed from the outlet of the microdevice, but there was no more fluid flowing out from the outlet of the microdevice after the time point of D, and the increasing rate of pressure difference at both ends of the microdevice changed at the turning point of D. The increasing rate of pressure difference after the time point of D was greater than that before the time point of D. Therefore, during the experiment, it is considered that the hydrate formed at time D had blocked the flow pores of the micro-packed bed device, so that TBAB solution could no longer enter the microdevice. The third stage from the time points of D to F can be considered as the static hydrate growth process. During the second stage from the time points of B to D, it can be observed that TBAB solution flew out from the outlet of the microdevice and hydrate gradually grew to fill the pore spaces of glass beads to cause the blockage of the microdevice. Therefore, in this experiment, it can be considered that the second stage of the hydrate formation process had a more significant impact on the variations of the porous structure and permeability of the micro-packed bed device.

Fig. 5 shows the initial typical positions of the pore blockage of the microdevice due to the hydrate formation. With the continuous flow and growth of hydrate, the positions of pore blockage further expanded to the central pore space area. In this process, the dynamic growth of hydrate tended to increase near the edges of the microdevice and filled the pores to cause blockage. Fig. 6 shows the microscopic images of the hydrate formation process in the micro-packed bed device under static condition at 1 °C. The subcooling condition was the same as the one for the dynamic flow condition. Compared with the Fig. 5, it can be seen from the Fig. 6 that the hydrate formation and growth were much slower than that under dynamic flow condition. The position distributions of hydrate nucleation and growth in the micro-packed bed device and the positions of pore blockage were more random. The amount of hydrate formation was also small, thus it was difficult to form the hydrate blockage zone where severe hydrate pore plugging existed in Fig. 5.

Even though the apparent flowrate was constant in the experiment, the flow resistance difference at different positions in the filling area could lead to local changes in the flow situation at different positions of the micro-packed bed device. The vortex might occur at the position where the flow velocity gradient was large. It was found that the flow velocity at the outlet of the microdevice was large. The occurrence of vortex caused by the large flow velocity gradient could increase the local disturbance, and reduce the local solution concentration drop caused by the hydrate formation. The relatively significant disturbance can strengthen the mass transfer for the hydrate formation process. The relatively fast flow can remove the heat generated during hydrate nucleation and growth, and therefore contribute to the faster nucleation and growth of hydrate at these positions.

3.3. *Effects of flowrate and temperature on the hydrate formation under dynamic condition*

In order to investigate the effect of flowrate on the on the hydrate formation under dynamic condition in the micro-packed bed device, four runs of hydrate formation experiments under dynamic flow conditions in a micro-packed bed device with different flowrates of 0.05, 0.10, 0.15 and 0.20 mL/min were carried out under the experimental temperatures of 1 and 3 °C, respectively. Fig. 7(a) and (b) show the variation curves of the pressure difference at both ends of the micro-packed bed with time in the second stage under various flowrates at the experimental temperatures of 1 and 3 °C, respectively. As shown in Fig. 7(a), as the flowrate increased, the slope of the pressure difference curve with time became steeper. When the flowrate increased from 0.05 to 0.10 mL/min, the curve slope changed the most significantly. When the flowrate increased from 0.10 to 0.20 mL/min, the increase of curve slope became less remarkable. As shown in Fig. 7(b), the dynamic formation and growth behaviors of hydrate at the experimental temperature of 3 °C presents similar trends with the ones at the experimental temperature of 1 °C. As the flowrate increased, the process of blockage in the micro-packed bed caused by the dynamic hydrate formation and growth could be accelerated. Comparing Fig. 7(a) and (b), it is found that the slope of the pressure difference curve caused by the dynamic hydrate formation at 1 °C was greater than that at 3 °C at the same flowrate. Therefore, at the same flowrate, the process of the pore blockage in the micro-packed bed under the condition of higher supercooling was more significant.

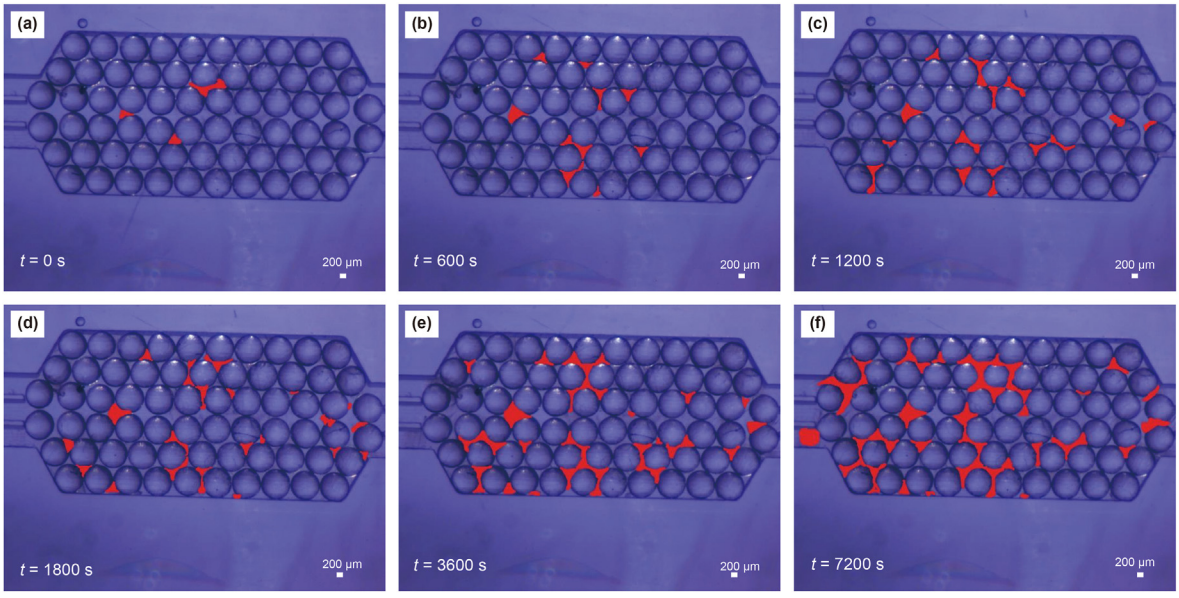

Fig. 6. Microscopic images of the hydrate formation process in the micro-packed bed device under static condition at 1 °C (The positions of hydrate formation in (**a**)–(**f**) are correspondingly marked with red sign).

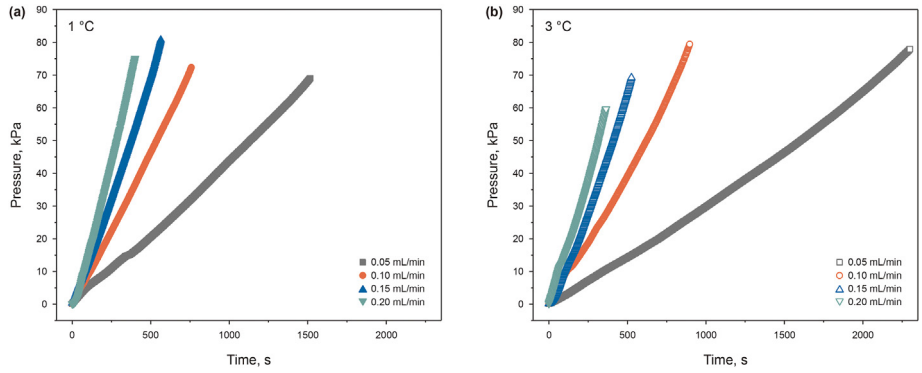

Fig. 7. Variation curves of pressure difference with time during hydrate formation under different flowrates of 0.05, 0.10, 0.15, 0.20 mL/min at (**a**) 1 °C and (**b**) 3 °C.

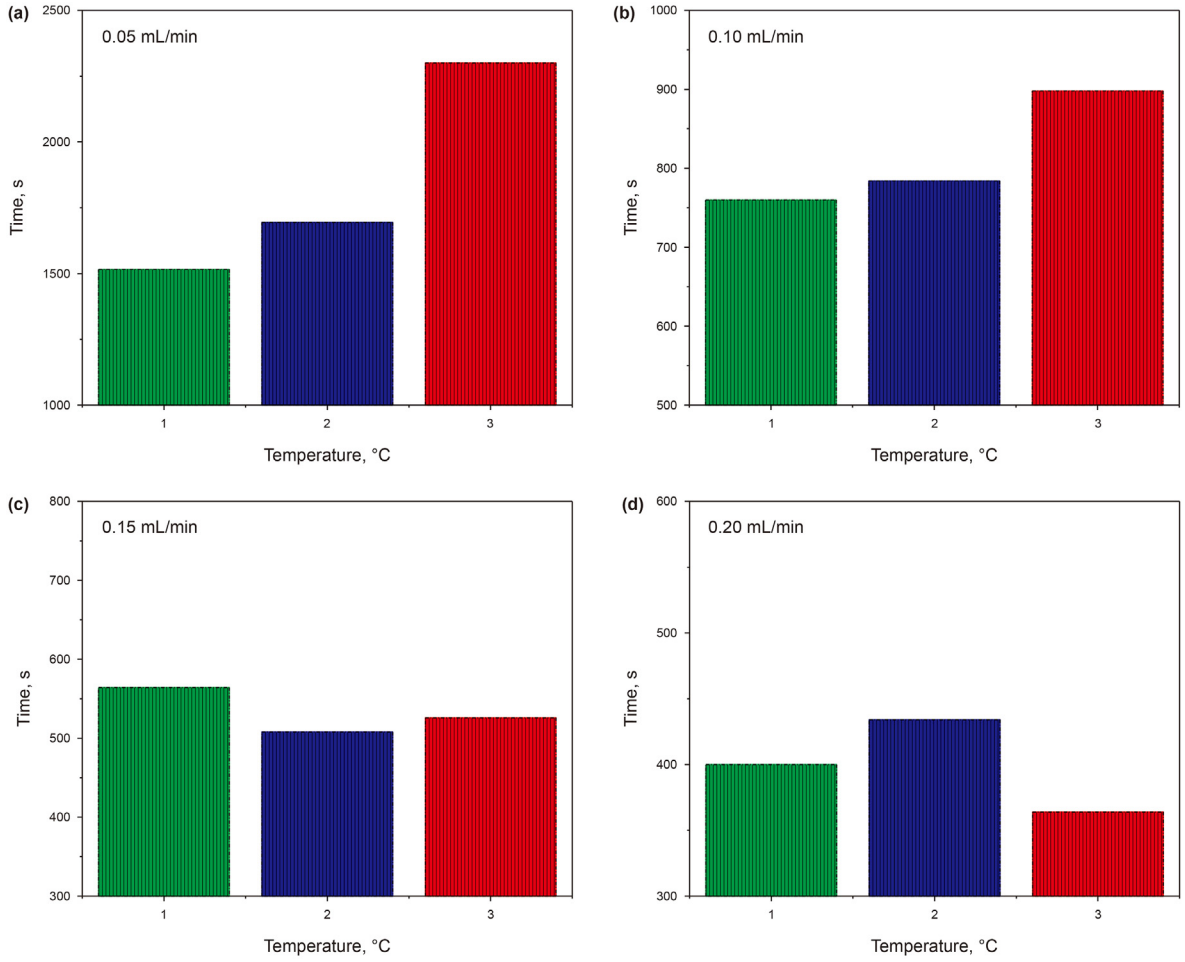

Fig. 8. Histograms of the total time of the second stage of dynamic hydrate formation under the flowrates of (**a**) 0.05 mL/min, (**b**) 0.10 mL/min, (**c**) 0.15 mL/min and (**d**) 0.20 mL/min at different experimental temperatures of 1, 2 and 3 °C.

Fig. 8(a)–(d) indicates the total times required for the dynamic hydrate formation in the second stage at different experimental temperatures of 1, 2 and 3 °C at the flowrates of 0.05, 0.10, 0.15 and 0.20 mL/min. At the same temperature, it is obvious that the duration for the hydrate formation in the second stage in the pore spaces decreased with the increase of the flowrate. Moreover, it was found that the total time of the second stage increased significantly with the increase of temperature, when the flowrate was low, such as at the flowrates of 0.05 and 0.10 mL/min. When the flowrate was 0.05 mL/min, the total times of the second stage were 1516 s at 1 °C and 2300 s at 3 °C. When the flowrate was increased to 0.10 mL/min, the total time of the second stage also increased with the temperature, but the increase was less significant, which was from 760 s at 1 °C to 898 s at 3 °C. When the flowrate was higher than 0.15 mL/min, the difference of the total durations of the second stage at different subcooling conditions at the same flow rate was small. Therefore, when the flowrate was low, the total time of the second stage for dynamic hydrate

formation could significantly affected by the temperature. As the flowrate increased, the influence of temperature became less remarkable. By analysis the findings from Figs. 7 and 8, the effect of flowrate on the hydrate formation and blockage in porous media could be more significant than that affected by the subcooling. The higher flowrate could contribute to the faster hydrate growth and more severe blockage, but the impact of subcooling became less significant, especially at the high flowrate. Thus, the blockage in porous media caused by hydrate formation might be more sensitive to the fluid flowrate than subcooling. This finding is in consistence with the one in literature (Aman et al., 2016).

4. Conclusions

The mechanism of hydrate growth behavior in porous media is of significance in the natural gas hydrate exploitation. A recently developed micro-packed bed device filled with glass beads was used to mimic the porous condition of the hydrate-bearing sediment. Due to the transparence of the microdevice used, the in-situ visual measurements were performed on the hydrate formation and growth processes in the pore space of the micro-packed bed device, under static and dynamic conditions. The effects of flowrate and subcooling on the dynamic hydrate formation were investigated.

Under static condition, two types of hydrate growth patterns in pores were in-situ visualized and identified in the micro-packed bed device, which were the grain-coating growth and pore-filling growth. For the dynamic flow experiments, the hydrate formation, growth, distribution habits and hydrate blockage phenomena in the pore spaces were visually captured. The impacts of flowrate and subcooling on the pressure variation and duration of the hydrate growth under dynamic flow condition in pores were monitored and analyzed. As the flowrate increased, the increase of the pressure with time was more significant, and the process of blockage in the micro-packed bed caused by the dynamic hydrate formation and growth could be accelerated. The pressure increase caused by the pore blockage due to the hydrate formation in the micro-packed bed under the condition of higher subcooling was more significant. The effect of flowrate on the duration of hydrate formation was remarkable. The less time required for the hydrate formation under dynamic flow with higher flowrate under the same subcooling. The impact of subooling on the duration of hydrate formation was more significantly at the lower flowrate, but it became less remarkable when the flowrate was higher.

Declaration of competing interest

The authors declare that they have no known competing financial interests or personal relationships that could have appeared to influence the work reported in this paper.

Acknowledgements

This work was supported by the National Natural Science Foundation of China (21808238, U19B2005, U20B6005, 22127812) and the National Key Research and Development Program of China (2021YFC2800902).

References

Abedini, A., Ahitan, S., Barikbin, Z., Soni, V., Ratulowski, J., Sinton, D., 2022. Past, present, and future of microfluidic fluid analysis in the energy industry. Energy Fuel. 36, 8578–8590. https://doi.org/10.1021/acs.energyfuels.2c00519.

Al-Rifai, N., Galvanin, F., Morad, M., Cao, E., Cattaneo, S., Sankar, M., Dua, V., Hutchings, G., Gavriilidis, A., 2016. Hydrodynamic effects on three phase micro-packed bed reactor performance – gold-palladium catalysed benzyl alcohol oxidation. Chem. Eng. Sci. 149, 129–142. https://doi.org/10.1016/j.ces.2016.03.018.

Alfi, M., Nasrabadi, H., Banerjee, D., 2016. Experimental investigation of confinement effect on phase behavior of hexane, heptane and octane using lab-on-a-chip technology. Fluid Phase Equil. 423, 25–33. https://doi.org/10.1016/j.fluid.2016.04.017.

Almenningen, S., Lysyy, M., Ersland, G., 2021. Quantification of CH_4 hydrate film growth rates in micromodel pores. Cryst. Growth Des. 21, 4090–4099. https://doi.org/10.1021/acs.cgd.1c00396.

Aman, Z.M., Di Lorenzo, M., Kozielski, K., Koh, C.A., Warrier, P., Johns, M.L., May, E.F., 2016. Hydrate formation and deposition in a gas-dominant flowloop: initial studies of the effect of velocity and subcooling. J. Nat. Gas Sci. Eng. 35, 1490–1498. https://doi.org/10.1016/j.jngse.2016.05.015.

Behera, U.S., Kumar, G., Sangwai, J.S., 2022. Pore-scale investigation and performance evaluation of SMART LowSal flooding for enhanced oil recovery from matured reservoirs using a lab-on-a-chip. Energy Fuel. 36, 8115–8127. https://doi.org/10.1021/acs.energyfuels.2c01009.

Cao, E., Brett, G., Miedziak, P.J., Douthwaite, J.M., Barrass, S., McMillan, P.F., Hutchings, G.J., Gavriilidis, A., 2017. A micropacked-bed multi-reactor system with in situ Raman analysis for catalyst evaluation. Catal. Today 283, 195–201. https://doi.org/10.1016/j.cattod.2016.06.007.

Cao, E., Radhakrishnan, A.N.P., Hasanudin, R.b., Gavriilidis, A., 2021. Study of liquid-solid mass transfer and hydrodynamics in micropacked bed with gas-liquid flow. Ind. Eng. Chem. Res. 60, 10489–10501. https://doi.org/10.1021/acs.iecr.1c00089.

Chen, W., Hartman, R.L., 2018. Methane hydrate intrinsic dissociation kinetics measured in a microfluidic system by means of in situ Raman spectroscopy. Energy Fuel. 32, 11761–11771. https://doi.org/10.1021/acs.energyfuels.8b02833.

Chen, Y., Gao, Y., Zhang, N., Chen, L., Wang, X., Sun, B., 2020. Microfluidics application for monitoring hydrate phase transition in flow throats and evaluation of its saturation measurement. Chem. Eng. J. 383, 123081. https://doi.org/10.1016/j.cej.2019.123081.

Dudek, M., Chicault, J., Øye, G., 2020. Microfluidic investigation of crude oil droplet coalescence: effect of oil/water composition and droplet aging. Energy Fuel. 34, 5110–5120. https://doi.org/10.1021/acs.energyfuels.9b03434.

Fani, M., Pourafshary, P., Mostaghimi, P., Mosavat, N., 2022. Application of microfluidics in chemical enhanced oil recovery: a review. Fuel 315, 123225. https://doi.org/10.1016/j.fuel.2022.123225.

Faridkhou, A., Larachi, F., 2014. Two-phase flow hydrodynamic study in micro-packed beds – effect of bed geometry and particle size. Chem. Eng. Process: Process Intensif. 78, 27–36. https://doi.org/10.1016/j.cep.2014.02.005.

Faridkhou, A., Tourvieille, J.N., Larachi, F., 2016. Reactions, hydrodynamics and mass transfer in micro-packed beds – overview and new mass transfer data. Chem. Eng. Process: Process Intensif. 110, 80–96. https://doi.org/10.1016/j.cep.2016.09.016.

Farsi, S., Olbrich, W., Pfeifer, P., Dittmeyer, R., 2020. A consecutive methanation scheme for conversion of CO_2 – a study on Ni_3Fe catalyst in a short-contact time micro packed bed reactor. Chem. Eng. J. 388, 124233. https://doi.org/10.1016/j.cej.2020.124233.

Gao, D.L., 2022. Focus on research advances in the natural gas hydrate resource evaluation: introduction to papers in the special section of Evaluation of Natural Gas Hydrate Resource Potential in the South China Sea. Petrol. Sci. 19, 1–2. https://doi.org/10.1016/j.petsci.2021.12.020.

Gunda, N.S., Bera, B., Karadimitriou, N.K., Mitra, S.K., Hassanizadeh, S.M., 2011. Reservoir-on-a-chip (ROC): a new paradigm in reservoir engineering. Lab Chip 11, 3785. https://doi.org/10.1039/C1LC20556K.

Guo, Y., Liu, F., Qiu, J., Xu, Z., Bao, B., 2022. Microscopic transport and phase behaviors of CO_2 injection in heterogeneous formations using microfluidics. Energy 256, 124524. https://doi.org/10.1016/j.energy.2022.124524.

Jafari, M., Jung, J., 2019. Salinity effect on micro-scale contact angles using a 2D micromodel for geological carbon dioxide sequestration. J. Petrol. Sci. Eng. 178, 152–161. https://doi.org/10.1016/j.petrol.2019.03.033.

Ji, Y., Hou, J., Zhao, E., Liu, C., Guo, T., Liu, Y., Wei, B., Bai, Y., 2021. Pore-scale study on methane hydrate formation and dissociation in a heterogeneous micromodel. J. Nat. Gas Sci. Eng. 95, 104230. https://doi.org/10.1016/j.jngse.2021.104230.

Li, X., Wang, C., Li, Q., Pang, W., Chen, G., Sun, C., 2022. Experimental observation of formation and dissociation of methane hydrate in a micromodel. Chem. Eng. Sci. 248, 117227. https://doi.org/10.1016/j.ces.2021.117227.

Li, X., Wang, C., Liang, S., Guo, X., Sun, Q., 2020. Experimental visualization of cyclopentane hydrate dissociation behavior in a microfluidic chip. Chem. Eng. Sci. 227, 115937. https://doi.org/10.1016/j.ces.2020.115937.

Lifton, V.A., 2016. Microfluidics: an enabling screening technology for enhanced oil recovery (EOR). Lab Chip 16, 1777. https://doi.org/10.1039/C6LC00318D.

Lin, Y.J., He, P., Tavakkoli, M., Mathew, N.T., Fatt, Y.Y., Chai, J.C., Goharzadeh, A., Vargas, F.M., Biswal, S.L., 2016. Examining asphaltene solubility on deposition in model porous media. Langmuir 32, 8729–8734. https://doi.org/10.1021/acs.langmuir.6b02376.

Lin, Y.J., Perrard, A., Biswal, S.L., Hill, R.M., Trabelsi, S., 2018. Microfluidic investigation of asphaltenes-stabilized water-in-oil emulsions. Energy Fuel. 32, 4903–4910. https://doi.org/10.1021/acs.energyfuels.8b00249.

Lv, J., Xue, K., Zhang, Z., Cheng, Z., Liu, Y., Mu, H., 2021. Pore-scale investigation of hydrate morphology evolution and seepage characteristics in hydrate bearing microfluidic chip. J. Nat. Gas Sci. Eng. 88, 103881. https://doi.org/10.1016/j.jngse.2021.103881.

Mahmoudzadeh, A., Fatemi, M., Masihi, M., 2022. Microfluidics experimental investigation of the mechanisms of enhanced oil recovery by low salinity water

flooding in fractured porous media. Fuel 314, 123067. https://doi.org/10.1016/j.fuel.2021.123067.
Makogon, Y.F., 2010. Natural gas hydrates – a promising source of energy. J. Nat. Gas Sci. Eng. 2, 49–59. https://doi.org/10.1016/j.jngse.2009.12.004.
Mohammadi, M., Mahani, H., 2020. Direct insights into the pore-scale mechanism of low-salinity waterflooding in carbonates using a novel calcite microfluidic chip. Fuel 260, 116374. https://doi.org/10.1016/j.fuel.2019.116374.
Mostowfi, F., Molla, S., Tabeling, P., 2012. Determining phase diagrams of gas-liquid systems using a microfluidic PVT. Lab Chip 12, 4381. https://doi.org/10.1039/C2LC40706J.
Moulijn, J.A., Makkee, M., Berger, R.J., 2016. Catalyst testing in multiphase micro-packed-bed reactors; criterion for radial mass transport. Catal. Today 259, 354–359. https://doi.org/10.1016/j.cattod.2015.05.025.
Muraoka, M., Yamamoto, Y., Tenma, N., 2020. Simultaneous measurement of water permeability and methane hydrate pore habit using a two-dimensional glass micromodel. J. Nat. Gas Sci. Eng. 77, 103279. https://doi.org/10.1016/j.jngse.2020.103279.
Oyama, H., Shimada, W., Ebinuma, T., Kamata, Y., Takeya, S., Uchida, T., Nagao, J., Narita, H., 2005. Phase diagram, latent heat, and specific heat of TBAB semiclathrate hydrate crystals. Fluid Phase Equil. 234, 131–135. https://doi.org/10.1016/j.fluid.2005.06.005.
Pandey, J.S., Strand, Ø., von Solms, N., Almenningen, S., Ersland, G., 2022. Novel pore-scale visualization during CO_2 injection into CH_4 hydrate-saturated porous media. Energy Fuel. 36 (18), 10552–10571. https://doi.org/10.1021/acs.energyfuels.1c03878.
Saadat, M., Yang, J., Dudek, M., Øye, G., Tsai, P.A., 2021. Microfluidic investigation of enhanced oil recovery: the effect of aqueous floods and network wettability. J. Petrol. Sci. Eng., 108647 https://doi.org/10.1016/j.petrol.2021.108647.
Sinton, D., 2014. Energy: the microfluidic frontier. Lab Chip 14, 3127. https://doi.org/10.1039/C4LC00267A.
Sivo, A., Galaverna, R.d.S., Gomes, G.R., Pastre, J.C., Vilé, G., 2021. From circular synthesis to material manufacturing: advances, challenges, and future steps for using flow chemistry in novel application area. React. Chem. Eng. 6, 756–786. https://doi.org/10.1039/D0RE00411A.
Sivo, A., Kim, T.K., Ruta, V., Luisi, R., Osorio-Tejada, J., Escriba-Gelonch, M., Hessel, V., Sponchioni, M., Vilé, G., 2022. Enhanced flow synthesis of small molecules by in-line integration of sequential catalysis and benchtop twin-column continuous chromatography. React. Chem. Eng. 7, 2650–2658. https://doi.org/10.1039/D2RE00242F.
Tetteh, J.T., Cudjoe, S.E., Aryana, S.A., Barati Ghahfarokhi, R., 2021. Investigation into fluid-fluid interaction phenomena during low salinity waterflooding using a reservoir-on-a-chip microfluidic model. J. Petrol. Sci. Eng. 196, 108074. https://doi.org/10.1016/j.petrol.2020.108074.
Tian, Y.S., Yang, Z.Q., Thoroddsen, S.T., Elsaadawy, E., 2022. A new image-based microfluidic method to test demulsifier enhancement of coalescence-rate, for water droplets in crude oil. J. Petrol. Sci. Eng. 208, 109720. https://doi.org/10.1016/j.petrol.2021.109720.
Wang, S., Cheng, Z., Liu, Q., Lv, P., Lv, J., Jiang, L., Song, Y., 2021. Microscope insights into gas hydrate formation and dissociation in sediments by using microfluidics. Chem. Eng. J. 425, 130633. https://doi.org/10.1016/j.cej.2021.130633.
Yin, Z., Linga, P., 2019. Methane hydrates: a future clean energy resource. Chin. J. Chem. Eng. 27, 2026–2036. https://doi.org/10.1016/j.cjche.2019.01.005.
Zhao, X., Feng, Y., Liao, G., Liu, W., 2020. Visualizing in-situ emulsification in porous media during surfactant flooding: a microfluidic study. J. Colloid Interface Sci. 578, 629–640. https://doi.org/10.1016/j.jcis.2020.06.019.
Zhao, X., Zhan, F., Liao, G., Liu, W., Su, X., Feng, Y., 2022. In situ micro-emulsification during surfactant enhanced oil recovery: a microfluidic study. J. Colloid Interface Sci. 620, 465–477. https://doi.org/10.1016/j.jcis.2022.04.045.